A Fully Automated Approach to Aortic Distensibility Quantification from Fetal Ultrasound Images

G Tarroni[1], S Visentin[2], E Cosmi[2], E Grisan[1]

[1] University of Padova, Padova, Italy
[2] University Hospital of Padova, Padova, Italy

Abstract

Intrauterine growth restriction (IUGR) is a fetal condition that can be assessed by estimating aortic intima-media thickness (aIMT) and pulse pressure (PP) from ultrasound (US) image sequences. Correct measurement of these quantities requires the identification of the aortic lumen contours at end-systolic (ES) and end-diastolic (ED) phases and the estimation of the undergoing change in diameter (aortic distensibility, ΔD). This analysis currently relies on tedious and error-prone manual tracing. Accordingly, we developed a fully-automated technique for lumen identification and segmentation, allowing direct aortic distensibility estimation, and tested it against manual analysis. The technique is based on convolution with a set of discriminative kernels learned from a training dataset, followed by segmentation based on anisotropic filtering and level-set methods. We tested this approach against manual analysis on 10 image sequences acquired from different subjects, and compared automatically and manually extracted lumen diameter values as well as ΔD values. Results suggest that the proposed technique is as accurate as manual analysis, and could thus serve as a basis for fully-automated aIMT and PP estimation.

1. Introduction

Intrauterine growth restriction is a condition determined by insufficient oxygen and nutrient delivery to the fetus affecting up to 10% of all pregnancies [1]. Epidemiological studies have long demonstrated the presence of a link between IUGR and increased rates of cardiovascular diseases during adulthood [2]. While the mechanisms underneath this link are still under debate, several recent studies indicate the presence of a direct connection based on the occurrence of primary cardiovascular changes in IUGR fetuses [3]. These early changes persist during childhood and adulthood, and might explain the increased predisposition to cardiovascular disease later in life. In particular, IUGR has been linked to an increase in aortic intima-media thickness (aIMT) [3] and in estimated pulse pressure (PP) [4]. Both these quantities can be measured at the fetal stage by means of ultrasound (US) images, improving IUGR evaluation and early cardiovascular risk assessment. For their correct measurement, it is necessary to identify the lumen contours at end-systolic (ES) and end-diastolic (ED) phases. Moreover, the estimation of the aortic distensibility (here defined as the difference ΔD in aortic lumen diameter between ES and ED) is directly required for PP estimation.

As of now, the identification of the aortic lumen boundaries throughout the cardiac cycle in US image sequences relies on tedious, error-prone and operator-dependent manual tracing. While several automated techniques have been recently presented [5][6], most of these methods require the manual identification of the images displaying a highly-contrasted aorta and the manual selection of a region-of-interest (ROI) around the aortic lumen. Our goal was to develop a fully-automated technique for lumen identification and segmentation from US images allowing direct aortic distensibility estimation, which could thus serve as a basis for aIMT and PP estimation.

2. Methods

2.1. Image Analysis

The main steps of the proposed technique are the three following ones:

A) Lumen identification. Lumen identification is performed by convolving each image with a set of discriminative kernels specifically designed to detect the aortic vessel in US images. This set of kernels is learned from a training dataset consisting of positive and negative image samples (i.e. containing and not containing the aortic lumen, respectively, see Fig. 1). The adopted kernels are linear weak classifiers combined together using an AdaBoost algorithm and the Parzen's windows method [7].

Let's consider a binary classification problem for which we have a set of N training data $\{\boldsymbol{x}_1, \ldots, \boldsymbol{x}_N\} \in X$ with associated labels $\{y_1, \ldots, y_N\} \in \{-1, 1\}$. In the case of

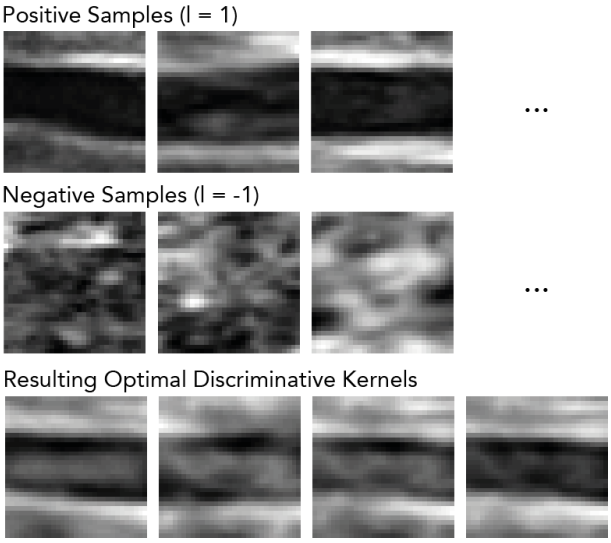

Figure 1. Sets of positive and negative samples used to learn the set of optimal discriminative kernels for aortic lumen detection.

image classification, $\boldsymbol{x}_i \in X \subseteq \mathbb{R}^{\mathbb{W}}$ is an image of W pixels. Let's denote with $H : \mathbb{R}^{\mathbb{W}} \rightarrow \{-1, 1\}$ a general classifier function. The optimal classifier is the one that minimizes the empirical error

$$Err(H) = -\frac{1}{N}\sum_{i=1}^{N}\int g_{\Sigma}(\boldsymbol{x}-\boldsymbol{x}_i)y_i\big(H(\boldsymbol{x})\big)d\boldsymbol{x} \quad (1)$$

where g_{Σ} is a Gaussian kernel with zero mean and covariance Σ (Parzen's windows method). The classifier H can be constructed as the combination of several *linear weak classifiers* h_m within a boosting framework:

$$H_M = \sum_{m=1}^{M}\alpha_m g_{\Sigma} * h_m(\boldsymbol{x}) \quad (2)$$

Each linear weak classifier writes as

$$h_m = sign(\gamma_{0,m} + \gamma_{1,m}\cdot\boldsymbol{x}) \quad (3)$$

with $\gamma_{0,m} \in \mathbb{R}$ and $\gamma_{1,m} \in \mathbb{R}^{\mathbb{W}}$. Having defined the weights introduced by the boosting procedure as $w(\boldsymbol{x}_i, y_i)$, with $\sum_{i=1}^{N} w(\boldsymbol{x}_i, y_i) = 1$, the empirical error associated to each classifier h_m writes as

$$Err_w(h_m) = \frac{1}{2} - \sum_{i=1}^{N} y_i w(\boldsymbol{x}_i, y_i) erf\left(\frac{\gamma_{0,m} + \gamma_{1,m}\cdot\boldsymbol{x}}{\sqrt{2\gamma_{1,m}^T\Sigma_i\gamma_{1,m}}}\right) \quad (4)$$

with erf being the error function. The optimal $\widehat{\gamma_{0,m}}$, $\widehat{\gamma_{1,m}}$ and α_m for each weak classifier yielding the minimum empirical error can be estimated following the iterative learning scheme described in Algorithm 1.

Algorithm 1 Learning scheme

1: Initialize $H_0(\boldsymbol{x}) = 0$ for all $\boldsymbol{x}_i \in X$.
2: Initialize $w(\boldsymbol{x}_i, y_i) = 1/N$ for all $i = 1, 2, \ldots, N$.
3: **for** $m = 1$ to M **do**
4: Estimate the coefficients of $\gamma_{0,m}$ and $\gamma_{1,m}$ of the linear weak classifier minimizing the empirical error $Err_w(h_m)$ using a gradient descent optimization.
5: Let
$$\alpha_m \leftarrow \frac{1}{2}\log\frac{1 - Err_w(h_m)}{Err_w(h_m)};$$
6: Update the weights
$$w(\boldsymbol{x}_i, y_i) \leftarrow w(\boldsymbol{x}_i, y_i)e^{-y_i\alpha_m h_m(\boldsymbol{x}_i)};$$
7: Update the auxiliary function $H_m = H_{m-1} + \alpha_m H_m$.
8: **end for**

Once the M weak learners have been estimated from the training set (see Fig. 1), each pixel of a given image I can be graded according to its likeliness to be within the lumen using the following equation:

$$H_I = \sum_{m=1}^{M}\alpha_m sign\left(\widehat{\gamma_{0,m}} + \widehat{\gamma_{1,m}} * I\right) \quad (5)$$

More in particular, in order to take into account potential differences in lumen size, I is resized with different scaling factors and convolved with the kernel associated with the highest α_m: the optimal scaling is the one yielding the highest convolution peak. Then, the scaled I is adopted within Eq. 5. The computed H_I highlights the aortic lumen, if visible, and potentially other spurious regions (see Fig. 2). The best candidate for the aortic lumen is selected through a process based on area and eccentricity of the associated best-fitting ellipse of each region. Finally, if the area of the best candidate is higher than a threshold, the corresponding region is considered part of the aortic lumen, otherwise a "no visible lumen" flag is raised.

B) Lumen segmentation. Lumen segmentation is performed within a ROI centered around the detected lumen region. The first step consists of anisotropic filtering [8], which aims at reducing the noise in the image while preserving the edges. Then, an edge-based level-set method (following the Malladi-Sethian formalism [9]) is applied, allowing the identification of the final lumen contours.

C) Distensibility estimation. Once the lumen contours have been identified for a number of consecutive frames covering sufficient cardiac cycles, a time curve for the lumen diameter (defined as the average distance between the lumen contours in each frame) is computed. A sinusoidal function is fitted on the time curve through simulated annealing: the distensibility ΔD is defined as the double of the amplitude of the best fitting sinusoid.

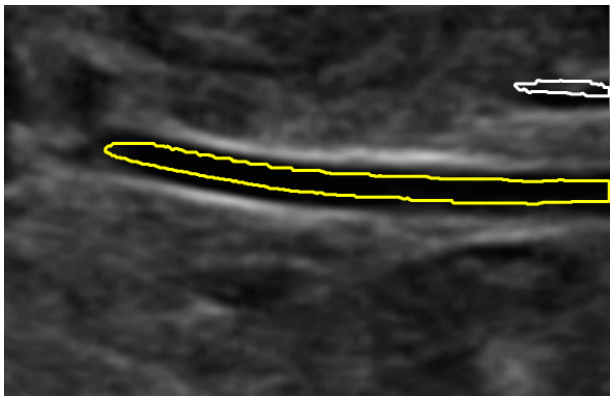

Figure 2. Lumen identification. Among the regions highlighted from the convolution of the image I with the set of discriminative kernels (white and yellow contours), the aortic lumen (yellow contour) is selected through considerations regarding area and eccentricity of the associated best-fitting ellipse of each region.

2.2. Image Acquisition

Image sequences were acquired on 20 subjects undergoing routine US examinations during pregnancy. The local ethical committee approved the study and all patients gave written informed consent. Fetal US data was acquired at a mean gestational age of 31 weeks (range 20 to 36 weeks) using a US machine equipped with a 5 MHz linear array transducer (Voluson E8, GE), with a 70° FOV, image dimension 720x960 px and a variable resolution between 0.05 and 0.1 mm. The localization of the abdominal aorta was performed in a sagittal view of the fetus at the dorsal arterial wall of the most distal 15 mm of the abdominal aorta, sampled below the renal arteries and above the iliac arteries. Gain settings were tuned to optimize image quality. After localization, the vessel was visualized in a maximal longitudinal section with an angle of insonation as close to 0° as possible. Mean frame rate was 48 Hz and acquisition times ranged between 5 and 10 s.

2.3. Performance Testing

The acquired sequences were divided into two groups: a training dataset (10 sequences, used to build the set of discriminative kernels) and a testing dataset (10 sequences, used to assess the accuracy of the proposed technique). An experienced interpreter visually examined the training dataset and manually traced ROIs containing a well-defined aortic lumen on 4 different frames per each sequence. A number of 20 positive samples was extracted from each frame by cropping the image within the traced ROI at uniformly spaced positions. The same number of negative samples was extracted by cropping the image outside the ROI in random positions. This procedure resulted in a set of 1600 samples. To reduce the number of unknown coefficients and allow the learning algorithm to converge, each sample was resized to a 15-by-15 px image. The resized samples are finally adopted to compute the set of discriminative kernels.

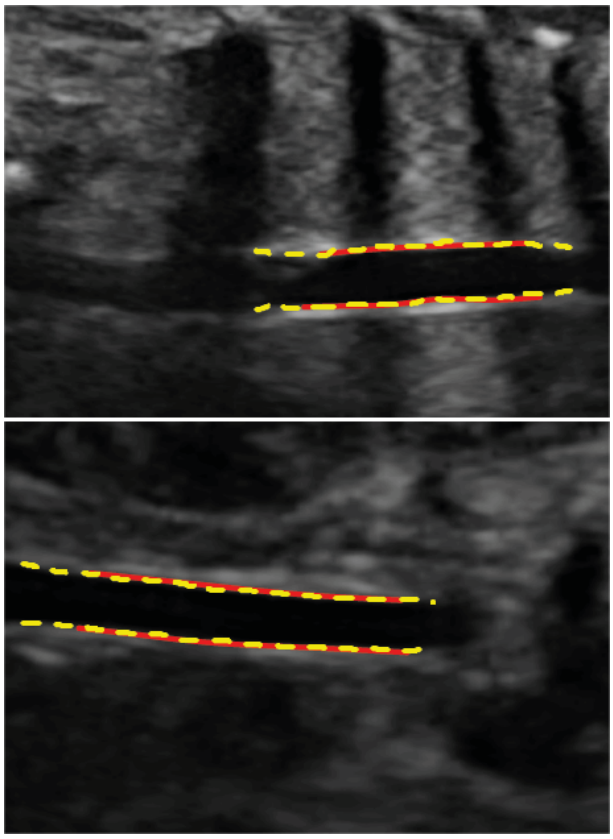

Figure 3. Visual comparisons between lumen contours identified using the proposed automated technique (yellow dashed lines) and manual tracing (red solid lines) on different sequences.

For each sequence in the testing dataset, an experience interpreter selected a range of consecutive frames (based on lumen visibility) covering at least 2 cardiac cycles. The proposed technique was applied to the selected frames, allowing the estimation of both frame-by-frame lumen diameter as well as sequence-by-sequence ΔD. The experienced interpreter manually performed the same analysis by tracing lumen contours on visually identified ES and ED frames (for a total of 54 frames). The accuracy of the proposed technique was evaluated using Person's correlation coefficient, linear regression and Bland-Altman analyses, comparing automatically and manually extracted lumen diameter values (computed on ES and ED frames) as well as ΔD values.

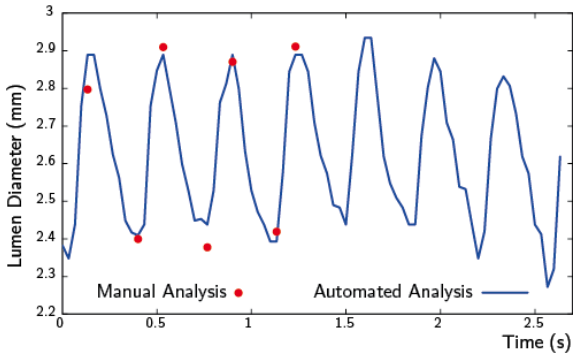

Figure 4. Visual comparison between an automatically extracted lumen diameter time curve (blue line) and manually obtained values (red dots) on a single sequence.

Table 1. Results of the quantitative analyses.

	Lumen Diameter	ΔD
R	0.94	0.74
Lin. Regr. - Slope	0.90	1.04
Lin. Regr. - Intercept	0.21 mm	0.08 mm
Bland-Altman - Bias	-0.21 mm	0.11 mm
Bland-Altman - Std	0.38 mm	0.13 mm
Mean Measured Value	4.54 mm	0.78 mm

3. Results

Fig. 3 shows examples of visual comparisons between automatically and manually identified lumen contours. Fig. 4 shows an example of the comparison between an automatically estimated lumen diameter time curve and manually obtained values. The results of the quantitative analyses for both lumen diameter and ΔD values are reported in Table 1.

4. Discussion and Conclusions

The estimation of intima-media thickness and pulse pressure in the abdominal aorta from US image sequences can improve IUGR assessment at an early stage. Unfortunately, the estimation of these two quantities relies on the identification of the lumen contours at ES and ED frames, which is currently performed through tedious and error-prone manual tracing.

In the present study, we described a fully-automated approach to lumen identification and segmentation, allowing direct aortic distensibility estimation, as a basis for aIMT and PP estimation, and we tested it against manual tracing. Qualitative analysis of the obtained results showed that the proposed technique is able to reliably delineate lumen contours even in complex cases, e.g. in images with low contrast-to-noise ratio or in the presence of other vessels (see Fig. 3). The quantitative comparisons between automatically obtained and manually extracted lumen diameter values (reported in Table 1, central column) suggest the high agreement between the proposed technique and manual tracing (R = 0.94). These findings are confirmed by the comparisons between automatically and manually estimated ΔD values: however, inter-technique agreement for this quantity is lower, potentially due to issues related to the sinusoidal fitting.

In conclusion, fully-automated aortic lumen contours delineation - and subsequent distensibility quantification - from US image sequences is feasible, and could serve as a basis for automated aIMT and PP estimation, allowing improved IUGR assessment.

References

[1] Severi FM, Rizzo G, Bocchi C, D'Antona D, Verzuri MS, Arduini D. Intrauterine growth retardation and fetal cardiac function. Fetal diagnosis and therapy 2000;15(1):8–19.

[2] Godfrey KM, Barker DJP. Fetal nutrition and adult disease. American Journal of Clinical Nutrition 2000;71(5 SUPPL.):1344S–52S.

[3] Visentin S, Grumolato F, Nardelli GB, Di Camillo B, Grisan E, Cosmi E. Early origins of adult disease: Low birth weight and vascular remodeling. Atherosclerosis 2014;237(2):391–399.

[4] Miyashita S, Murotsuki J, Muromoto J, Ozawa K, Yaegashi N, Hasegawa H, Kanai H. Measurement of Internal Diameter Changes and Pulse Wave Velocity in Fetal Descending Aorta Using the Ultrasonic Phased-Tracking Method in Normal and Growth-Restricted Fetuses. Ultrasound in Medicine Biology 2015;41(5):1311–1319.

[5] Veronese E, Tarroni G, Visentin S, Cosmi E, Linguraru MG, Grisan E. Estimation of prenatal aorta intima-media thickness from ultrasound examination. Physics in medicine and biology 2014;59(21):6355–71.

[6] Tarroni G, Visentin S, Cosmi E, Grisan E. Near-automated quantification of prenatal aortic intima-media thickness from ultrasound images. In Computing in Cardiology2014; 313–316.

[7] Vedaldi A, Favaro P, Grisan E. Boosting Invariance and Efficiency in Supervised Learning. In 2007 IEEE 11th International Conference on Computer Vision. IEEE2007; 1–8.

[8] Tarroni G, Tersi L, Corsi C, Stagni R. Prosthetic component segmentation with blur compensation: a fast method for 3D fluoroscopy. Medical biological engineering computing 2012;50(6):631–40.

[9] Sethian JA. Level set methods and fast marching methods. Cambridge University Press 1999;1–33.

Address for correspondence:

Giacomo Tarroni, PhD
Via G. Gradenigo 6/B, 35131 Padova, Italy
giacomo.tarroni@dei.unipd.it